Proceedings of ASME Turbo Expo 2011
GT2011
June 6-10, 2011, Vancouver, British Columbia, Canada

GT2011-45268

MEASUREMENTS AND ANALYSIS OF BLUFF-BODY FLAME RESPONSE TO TRANSVERSE EXCITATION

Vishal Acharya
Georgia Institute of Technology
Atlanta, GA, USA

Benjamin Emerson
Georgia Institute of Technology
Atlanta, GA, USA

Ulises Mondragon
Energy Research Consultants
Laguna Hills, CA, USA

Christopher Brown
Energy Research Consultants
Laguna Hills, CA, USA

Dong-Hyuk Shin
Georgia Institute of Technology
Atlanta, GA, USA

Vincent McDonell
Energy Research Consultants
Laguna Hills, CA, USA

Tim Lieuwen
Georgia Institute of Technology
Atlanta, GA, USA

ABSTRACT

This paper describes the interaction of bluff body stabilized flames with 450 Hz transverse acoustic standing waves at flow velocities up to 100 m/s. Two different modes of acoustic excitation were applied, corresponding to pressure and velocity nodes along the bluff body centerline. Time resolved measurements of both the flame front and velocity field were obtained. These measurements of the spatio/temporal distribution of the flame front were compared to level set equation prediction using the measured velocity field as an input, or vice-versa. These studies show that the measured flame response characteristics are qualitatively captured in almost all cases, with quantitative differences varying from values that are quite low to a factor of two. A key implication of this work is that the important features of the unsteady flame dynamics at high velocity, vitiated flow conditions are understood, but further work is needed for quantitative prediction.

NOMENCLATURE

D	=	bluff body diameter
f_o	=	forcing frequency
G	=	isoscalar contour variable
K	=	non-dimensional convective disturbance velocity
$\bar{L}, L'$	=	mean and fluctuating flame edge position
s_L	=	laminar flame speed
U,V	=	mean components of axial and transverse flow velocity
u',v'	=	fluctuating component of axial and transverse flow velocity
U_0	=	characteristic mean flow velocity
U_c	=	convective velocity of a disturbance
u'_n	=	fluctuating flow velocity normal to the flame
u'_a	=	acoustic component of fluctuating flow velocity normal to the flame
u'_v	=	vortical component of fluctuating flow velocity normal to the flame
U_t	=	flow velocity tangential to the flame
$\varepsilon_a\ \varepsilon_v$	=	non-dimensional disturbance amplitude of acoustic and vortical fluctuations
θ	=	mean flame front angle
λ_c	=	convective wavelength, = U_o/f_0

INTRODUCTION

This paper describes the response of bluff body stabilized flames to transverse acoustic waves. These interactions involve coupling between acoustic oscillations, hydrodynamic flow instabilities in the shear layers and bluff body wake, and unsteady heat release [1-6], as shown in Figure 1. This study follows prior work by our groups on the related problem where the flame is perturbed by longitudinal acoustic waves [7-8]. A key challenge of the present work was extending these prior studies to high velocity, vitiated flows that are practically encountered in realistic devices.

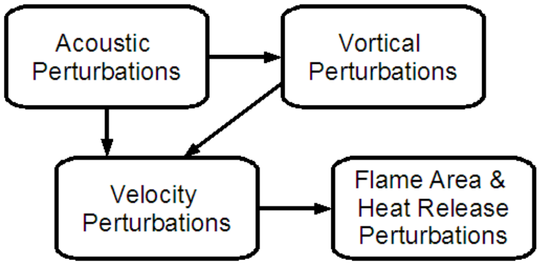

Figure 1. Physical processes by which longitudinal and transverse flow oscillations can lead to flame area (and hence heat release) oscillations.

In order to fix some ideas, we next discuss key features of the flow field that is disturbing the flame. As discussed in earlier work [8], hydrodynamic instabilities lead to two important sources of convecting vortical velocity disturbances. The first is the separated shear layer, which rolls up due to the Kelvin-Helmholtz instability, leading to tightly concentrated regions of vorticity. Under certain circumstances, the entire wake is absolutely unstable, leading to the roll-up of the shear layers into large scale vortical structures that are asymmetrically staggered about the flow centerline, leading to a sinuous flow pattern [8] referred to as the Von Karman vortex street.

In addition, the flame is directly perturbed by the transverse acoustic velocity of the incident wave. These transverse oscillations are axially uniform in phase along the flame for the experiments reported here. This implies that the total disturbance velocity field is a superposition of acoustic disturbances propagating at the speed of sound in the transverse direction and axially uniform in phase, and vortical disturbances that consist of both axial and transverse velocity disturbances with significant axial phase variation. As shown in a companion paper, this leads to distinctive interference patterns in the unsteady velocity field at the flame [9]. The associated flame response is influenced by several disturbance field parameters: 1) the spatial amplitude of acoustic and vortical disturbances, $\varepsilon_a = u_a'/U_o$ and $\varepsilon_v = u_v'/U_o$, 2) the angular frequency of disturbance, ω, and 3) the phase speed of each disturbance. These parameters themselves are influenced by geometry and flame angle.

This distinction between acoustic and vortical disturbance characteristics is important for understanding the flame dynamics [10-11]. A number of studies of velocity-coupled flame response have noted the importance of the spatial character of the disturbance field, due to flame interference phenomenon [7, 11-14]. The level set equation is an important equation used in describing premixed flame front dynamics [15]:

$$\frac{\partial G}{\partial t} + \vec{u}\cdot\nabla G = s_L\left|\nabla G\right| \tag{1}$$

In this equation, the flame position is implicitly described by the parametric equation $G(\vec{x},t)=0$. Also, $\vec{u}=\vec{u}(\vec{x},t)$ and s_L denote the flow field just upstream of the flame and laminar flame speed, respectively. In the unsteady case, the flame is being continually wrinkled by the unsteady flow field, $\vec{u}\,'$.

Assuming that the flame position is a single valued function of the transverse coordinate, the instantaneous flame position can be written as:

$$G(x,y,t) = L(x,t) - y = 0 \tag{2}$$

where L is shown in Figure 2. Hence, from Eq.(1), the instantaneous flame position, L, is given by:

$$\frac{\partial L}{\partial t} + u\frac{\partial L}{\partial x} - v = s_L\sqrt{\left(\frac{\partial L}{\partial x}\right)^2 + 1} \tag{3}$$

This equation describes the spatial and temporal distributions of the flame position which can be related directly to its surface area. In this formulation, the effect of transverse and longitudinal velocity perturbations on the flame are captured through the (u, v) terms.

Because Eq.(3) is a nonlinear partial differential equation, with special properties, it does not warrant a direct analytical solution or an analytically tractable description. In order to facilitate some insight, the equation is linearized to analyze the flame edge fluctuations. Prior work has shown that this assumption of linearity is very good near the attachment point [7]. Nonlinear effects grow in prominence with increasing amplitude of excitation and downstream distance [7].

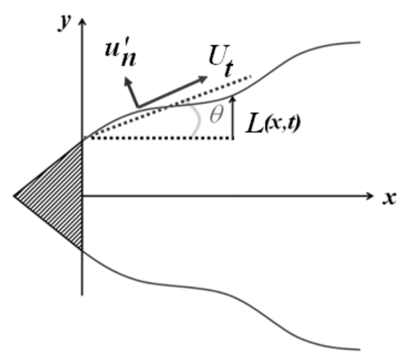

Figure 2. Co-ordinate system and schematic of a bluff-body stabilized flame.

$$\begin{aligned} &u(x,t) = U(x) + u'(x,t), v(x,t) = V(x) + v'(x,t) \\ &L(x,t) = \bar{L}(x) + L'(x,t) \end{aligned} \tag{4}$$

Using the decomposition of Eq.(4), in Eq.(3), and linearizing, we obtain the following:

$$U(x)\sin\theta(x) - V(x)\cos\theta(x) = s_L \tag{5}$$

$$\frac{\partial L'}{\partial t} + U_t(x)\cos\theta(x)\frac{\partial L'}{\partial x} = \frac{u_n'(x,t)}{\cos\theta(x)} \tag{6}$$

where

$$\frac{d\bar{L}(x)}{dx} = \tan\theta(x) \tag{7}$$

$$U_t(x) = U(x)\cos\theta(x) + V(x)\sin\theta(x) \tag{8}$$

$$u_n'(x,t) = v'(x,t)\cos\theta(x) - u'(x,t)\sin\theta(x) \qquad (9)$$

The terms u'_n, U_t, θ, and L are also depicted in Figure 2. Equation (6) describes axial flame wrinkle propagation on the left side and the excitation of disturbances on the right. The tangential component of the mean velocity, U_t equals the axial velocity at which these flame wrinkles propagate along the flame. The wrinkles are generated by the normal component of the fluctuating velocity, u'_n, shown in Eq.(9). Note that the presence of the $cos(\theta)$ terms is an artifact of the co-ordinate system, and equals the angle between the chosen co-ordinate system and a local flame-fixed co-ordinate system.

The rest of this paper consists of experimental analysis of the flow field and flame front response characteristics of transversely forced flames, quantified by L' in Eq.(6). These measured flame and flow field characteristics are then compared to theoretical predictions derived from the linearized level set equation. This work complements related studies from our groups on transversely forced swirl flames [16], longitudinally forced swirl flames [17-18] and longitudinally forced bluff body flames [8]. This work is closely coupled to a companion study [9], which provides more details on the experimental facility and the data records that was obtained. This paper focuses on comparisons between measurements and level set based predictions of the flame and flow field.

DETAILS OF EXPERIMENT AND DATA VALIDATION MODEL

Experimental Setup and Data Post Processing

Experiments were conducted in a premixed, atmospheric test rig (see Figure 3) operated in a vitiated mode. This facility is further detailed in Ref. [9]. Two different flow velocities at the bluff body are studied: 50 m/s and 100 m/s. The inlet temperature into the test section is studied at 477K, 644K and 755K. Two different fuel/air ratio profiles were generated; these were nominally uniform and “rich on center”.

The test section consists of a chamber measuring 61 cm by 30.5 cm by 7.6 cm and was designed with similar guidelines as a related facility developed for transverse forced swirl flames [16]. The bluff body is triangular with a diameter D = 3.2 cm, and is 3.2 cm long. The leading edge half-angle is 17.5 degrees and is rounded off with a radius of 79.4 mm. The flow is along the 30.5 cm dimension of the test section. The box is designed for transverse acoustic forcing, with each side of the 61 cm dimension equipped with 3 speakers, and each speaker mounted on a tube. The transverse resonant frequency of this setup is approximately 450 Hz, which is also the frequency at which all data reported in this paper were obtained. Speakers are arranged with three on each side of the test section box, and can be operated in phase or out of phase. These two different modes of operation nominally lead to an unsteady velocity minimum/pressure maximum or vice-versa, respectively, on centerline.

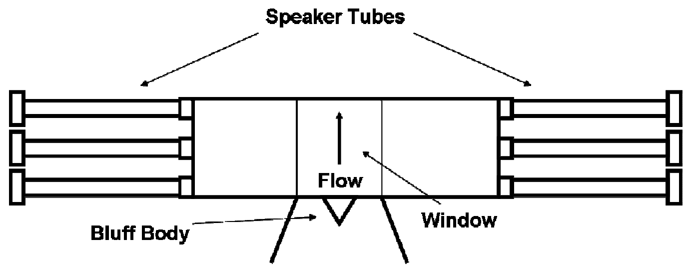

Figure 3. Schematic of the experimental rig.

Flame dynamics are determined from line of sight flame luminosity, recorded with a Vision Research Phantom 7 high speed video camera. Images captured for edge tracking analysis are unfiltered, integrating light over wavelengths from λ=*350-1050nm.* In all cases, the camera is operated at a sampling frequency of 3150 frames per second, with an exposure time of 300 microseconds.

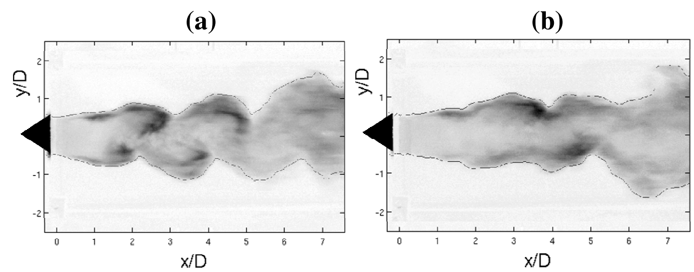

Figure 4. Flame image and flame edges at two contrasting flow conditions: (a) 50 m/s, 477K, out of phase forcing and (b) 50 m/s, 477K, in phase.

Flow dynamics are captured using phase locked Particle Image Velocimetry (PIV). The PIV system utilizes a Litron laser operating at nominally 80 mJ per pulse at 15 Hz for each of the two lasers. The time between the two pulses for a given image pair was 10 µs for 50 m/s cases and 5 µs for 100 m/s cases. Details on the PIV system and optical equipment used are provided in the companion paper [9].

Flame Image Processing

High speed, line-of-sight movies were obtained of the acoustically forced flames. Typical images are shown in Figure 4. Note the qualitative difference in flame behavior between the in-phase and out-of-phase forced flames. In order to quantify the spatio-temporal flame dynamics, the flame edge position $L(x,t)$ is extracted. This procedure works well near the bluff body, but uncertainties grow monotonically with downstream distance since the line of sight images become increasingly diffuse due to the growing three-dimensionality of the flame front. This is indicated by the uncertainties shown as error-bars in flame position, L', that are described later.

The time series $L(x,t)$ is extracted at the sampled temporal points at all axial stations for both flame branches. These time series are Fourier transformed to obtain spectra of the flame edge motion, $L(x,f)$ like that shown in Figure 6. From the Fourier transform, the axial dependence on the magnitude and phase of flame edge motion at a particular frequency are determined. Of particular interest is the response at the forcing frequency, f_0=450 Hz (or $f/f_0=1$ in Figure 6), where the greatest magnitude of flame edge motion is expected.

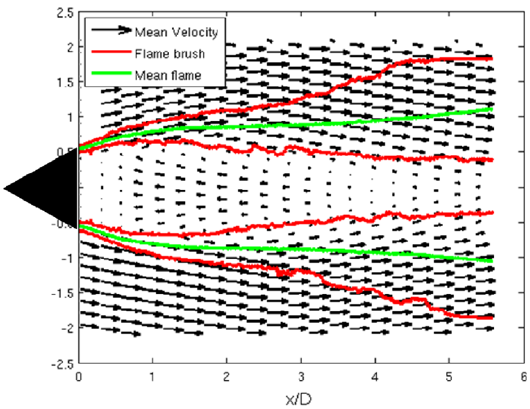

Figure 5. Sample mean velocity fields obtained from PIV with flame brush and mean flame position overlaid. Conditions shown were 755K approach flow with 100 m/s lip velocity, 450 Hz out of phase forcing.

PIV Processing

PIV data was phase-locked to the acoustic driving cycle. The resulting velocity fields were phase-averaged [9] and fit to sine waves to determine the velocity amplitude and phase. Time averaged and disturbance velocity values are needed as inputs to solve for the flame position, in Eq.(6). Note that velocity disturbance values needed for the level set equation are at the instantaneous flame position, which is clearly moving with respect to the velocity field. We estimated the velocity values at a given axial position from locations just upstream of the flame brush, as shown in Figure 5.

Model for Data Validation

This section describes the procedure used to compare linearized flame and flow field response measurements and predictions. The frequency domain representation of Eq.(6) is used in the validation studies (shown in Eq.(10)).

$$i2\pi\left(\frac{L'}{\lambda_c}\right)+\frac{U_t}{U_0}\cos\theta\frac{d}{d\left(x/\lambda_c\right)}\left(\frac{L'}{\lambda_c}\right)=\frac{1}{\cos\theta}\left(\frac{\hat{u}_n'}{U_0}\right) \quad (10)$$

Using the above equation, there are two ways in which data and measurements can be compared. First, the measured flame edge data, L', can be used as an input to the left side of the equation to predict a value for the normal velocity component, u'_n. This is compared with the corresponding value measured using PIV, as shown in Eq.(11). From a practical point of view, prediction of flame position from a known (or assumed) velocity field is the more interesting scenario. However, this first comparison approach is more straightforward since it directly relates the *local* flame position and slope to the *local* velocity field.

$$\overbrace{\frac{1}{\cos\theta}\left(\frac{\hat{u}_n'}{U_0}\right)}^{predicted}=i2\pi\underbrace{\left(\frac{L'}{\lambda_c}\right)}_{measured}+\underbrace{\frac{U_t}{U_o}}_{measured}\cos\theta\underbrace{\frac{d}{d\left(x/\lambda_c\right)}\left(\frac{L'}{\lambda_c}\right)}_{measured} \quad (11)$$

Alternatively, the measured fluctuating velocity field is used as an input on the right side of Eq.(10) to predict the flame edge response. This is given by:

$$\overbrace{\left(\frac{L'}{\lambda_c}\right)}^{predicted}=\exp\left(-\int\underbrace{\frac{i2\pi}{\left(U_t/U_0\right)\cos\theta}}_{measured}d\left(\frac{x}{\lambda_c}\right)\right) \\ \times\int_{s=0}^{s=\frac{x}{\lambda_c}}\left[\underbrace{\frac{1}{\cos\theta(s)}\frac{\hat{u}_n'(s)}{U_0}}_{measured}\exp\left(\int\frac{i2\pi ds}{\underbrace{\left(U_t/U_0\right)\cos\theta}_{measured}}\right)\right]ds \quad (12)$$

This is the more interesting comparison because generally it is the flame position which must be calculated. However, from a validation point of view, this approach is problematic because the predicted flame position is a convolution of velocity field disturbances of all upstream positions. This is an issue because errors in measurement at one point (i.e., near the bluff body) corrupt the predicted flame position not only at that point, but also at all downstream positions.

Given that this is a comparison of linearized flame response characteristics, we can expect these calculations to increasingly grow in error as nonlinear effects grow. It is known that flame response nonlinearity grows monotonically with downstream distance from the flame holder and disturbance amplitude. This point should be recalled in the ensuing comparisons of theory and experiment at downstream locations.

REPRESENTATIVE RESULTS AND DISCUSSION

Typical forced flame position spectra are shown in Figure 6 at six downstream locations. The envelope of the flame response at $f = f_o$, its sub harmonic and two higher harmonics are drawn in. At locations closer to the bluff body (located at x/λ_c=0), the flame responds mainly at the frequency of excitation, f_o. Moving downstream, the response at $f = f_o$ grows, reaches a maximum, and then begins to decay. This behavior is due to the growth and decay of the underlying flow structures as well as the propagation of the flame, which tends to smooth out the wrinkles. These results are quite similar to our observations on lower velocity and longitudinally excited flames.

The rest of this paper focuses on flame response characteristics only at $f = f_o$. Figure 7 presents typical gain and phase results at several flow conditions. In order to increase physical insight into the phase results, the phase has been converted into an effective axial propagation velocity, U_{cf}, using the relation:

$$U_{c,f}=\frac{360\cdot f_0}{d\phi/dx}$$

A full cataloguing of all results is contained in the companion paper [9].

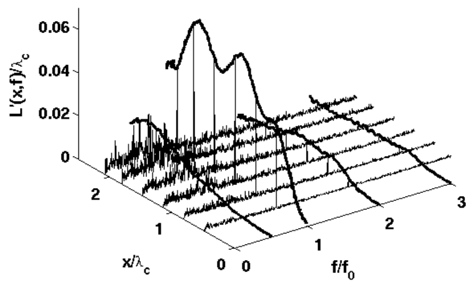

Figure 6. Spectrum of flame sheet fluctuations at different downstream locations (50 m/s, 477K). The *x*-coordinate is the downstream distance with *x*=0 located at the bluff body trailing edge and f_o is the acoustic forcing frequency. The flame response envelope is outlined at f_o, $f_o/2$, $2f_o$, and $3f_o$.

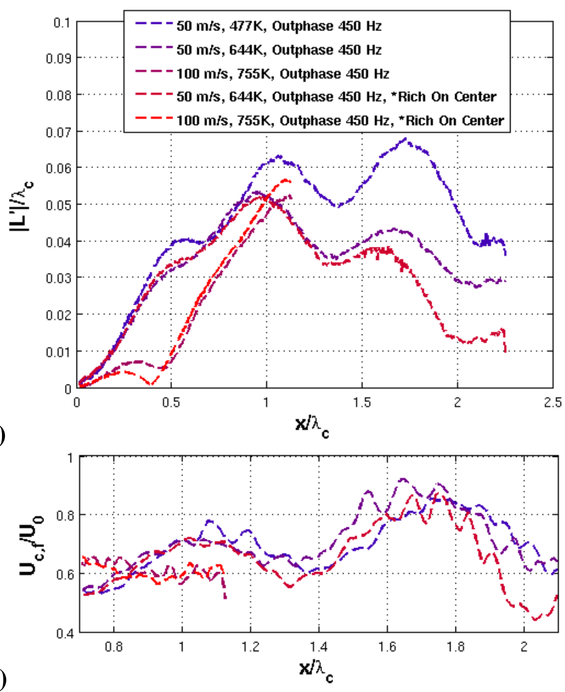

(a)

(b)

Figure 7. Overlays of flame response for 450 Hz out of phase forcing at all flow conditions, showing a) gain, b) convective velocity.

Most curves show similar qualitative behavior for both gain and phase. They are also quite similar in character to prior data we have obtained in longitudinally forced flames from this same facility and in much lower velocity flames [7]. Specifically, the gain results increase linearly in the bluff body near-field, peak farther downstream, and then begin to decay. Most of these responses show an interference pattern, manifested as spatial undulations in the gain. Comparison of these data with model results shows that capturing these interference patterns requires inclusion of both vortical and acoustic disturbances.

The higher velocity cases sometimes show a different behavior than previously reported in our studies. This is clear in Figure 7(a). The flame response magnitude rises with downstream distance, peaks, falls to nearly zero at about half a convective wavelength downstream, and then grows monotonically. These results can be captured theoretically, which indicates that they are due to the comparable magnitudes of acoustic and vortical disturbances in these cases. These two waves have very different axial phase characteristics, leading to this "node" in flame response. It should be emphasized that such nodes in flame wrinkling amplitude have been reported in prior studies where the axial location of the bluff body was oscillated [19].

Figure 7(b) plots convective velocities of the flame wrinkle, not to be confused with the propagation speed of the vortical disturbance or mean flow velocity. These measured flame wrinkle convection velocities are generally in the range of $0.5< U_{c,f}/U_o<0.9$.

COMPARISON WITH MODEL

Figure 8 to Figure 17 shows comparisons using both validation studies. The validation studies for flame edge as input, (a) and (b) in each of the figures, are shown together with the validation studies with velocity as input, (c) and (d) in each of the figures, in order to facilitate the discussion of each others' features in the comparisons. The measurements for both velocity and flame edge are prone to large errors close to the edge of their respective image boundaries due to their proximity to the edge of the laser sheet. For the first study, where the flame edge data is used as input, the predictions use only local data and hence the comparisons could be done by ignoring data at the edges of the data field. But, in the case of the velocity field as input, the flame edge is predicted by an integration starting at the bluff-body. Since the data in this region is prone to errors, all $x/\lambda_c<0.1$ points are extrapolated from points close to $x/\lambda_c>0.1$ based on a polynomial fit of their behavior. These extrapolated values are shown on the plots as separate symbols. These extrapolated values are not used for the *local* comparison in the velocity field validation study.

In general, the validation studies show good qualitative comparisons in most cases and good quantitative agreement in some cases. Relatively significant quantitative differences also occur in some cases. These comparisons are discussed next.

Experiment/theory comparisons are uniformly better in the high velocity and/or out of phase forcing cases, than for low velocity and/or in-phase cases. We believe that this reflects predictive errors associated with the velocity being extracted upstream of the flame brush, as opposed to the instantaneous or time averaged flame location. In the low velocity cases, the flame brush reaches farther upstream of the mean flame edge. As the width of the brush increases, the region upstream of the brush where the velocity data is extracted is farther from the mean flame. This effect is reduced for higher velocity cases where the mean flame and upstream edge of the brush are much closer. This interpretation for the deviations from theory and data is supported by comparison of the in- and out- of phase forcing cases. Predictions and measurements are uniformly better for the out of phase forcing than their in-phase counterparts. In the case of out-of phase forcing, the fluctuating velocity field follows a bulk rigid body like motion near the flame. This means that the velocity field is nearly uniform spatially and, hence, the unsteady velocity at the location upstream of the upstream brush is a closer representation of the same at the mean flame than for in phase forcing. As such, further effort will be expended in future studies in extracting the velocity fluctuations at the flame front itself.

The spatial interference patterns in the amplitude and phase are a prominent feature in these plots, such as those shown in Figure 9. The flame response amplitude shows interference patterns with 2 different length scales in most cases, behavior which is consistent with the presence of both acoustic and vortical disturbances in the underlying disturbance field. Although not shown here for reasons of space, analysis of the velocity data suggest that ε_a~$(0.4\text{-}0.6)\varepsilon_v$ typically [9].

We consider next several specific results, starting with Figure 9. Both velocity and flame position validation studies show that the interference patterns, such as crests and troughs, are captured by the model. The phases of both the predicted velocity and flame position phase are also captured well. The amplitudes in both studies are clearly different, by a factor of up to about two. Similar types of results are also evident in Figure 8.

Closer examination of cases with different behaviors between theory and model emphasize the coupling of gain and phase in predicting either quantity. For example, Figure 13(a) shows that the magnitude and spatial interference trends are qualitatively similar, but shifted in space relative to each other. This shift can be seen in the phase comparison of Figure 13(b) where the phase trend is similar, but there is a uniform phase shift. Although the magnitude is well captured, the shift in phase plays a major role in the prediction of the flame edge as can be seen in Figure 13(c).

Analysis of Figure 17 also leads to similar conclusions. Although the amplitude comparison of Figure 17(a) shows that the trends are similar, the quantitative comparison shows a discrepancy in the region close to, but less than, x/λ_c~0.5. This is also the region where the phase trend in Figure 17(b) shows a large discrepancy. While the measured phase trend shows a rapid drop in phase, the predicted trend shows a rapid rise in phase (which would correspond to a disturbance with a phase speed pointed in the opposite direction of the flow). Similar conclusions can be drawn from the measured flame edge response shown in Figure 17(c). Here we can see a node in the flame response close to x/λ_c~0.5. The important controlling parameter for the amplitude behavior near the node is then controlled by the phase characteristics in this region.

These analyses are ongoing, where we are also utilizing specified functional forms of u'_n, in order to assess the sensitivity of the flame predictions to the disturbance field characteristics.

Uniform mixture, 50 m/s, 477K approach flow,
In phase forcing

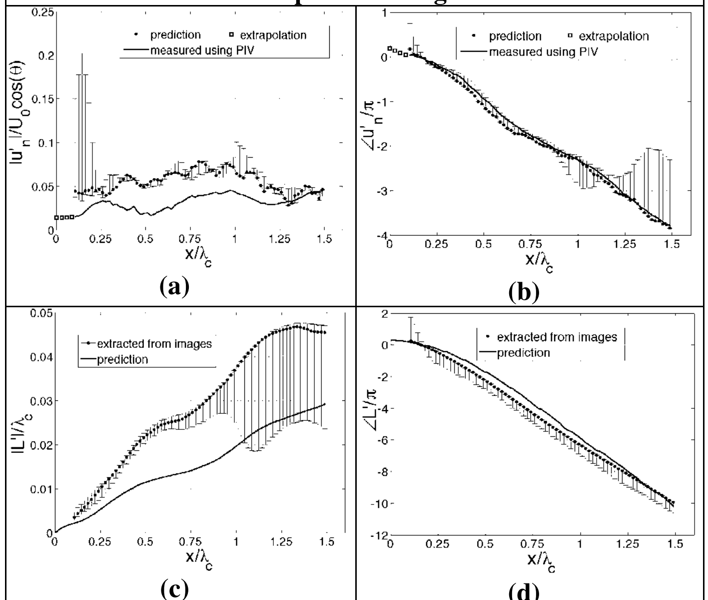

Figure 8. – Velocity validation study using Eq.(11) with flame edge as input : (a) amplitude comparison, (b) corresponding phase comparison; Flame edge validation study using Eq.(12) with velocity as input : (c) amplitude comparison, (d) corresponding phase comparison.

Uniform mixture, 50 m/s, 477K approach flow,
Out of phase forcing

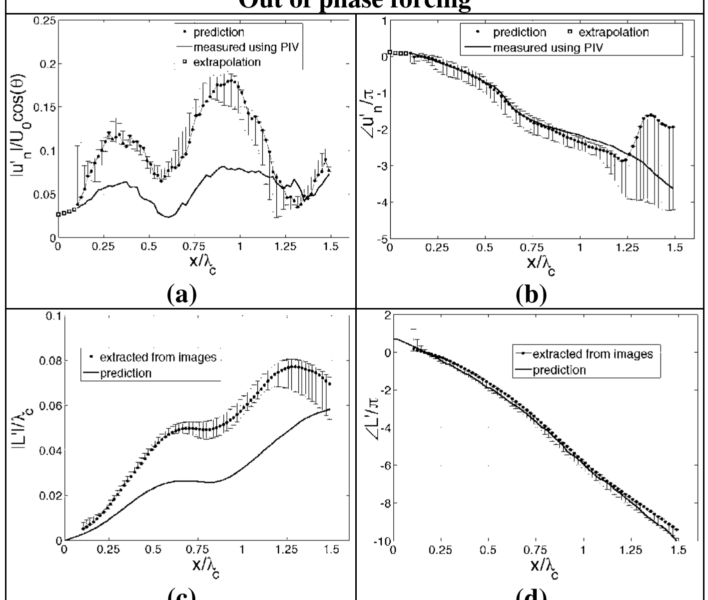

Figure 9. Velocity validation study using Eq.(11) with flame edge as input : (a) amplitude comparison, (b) corresponding phase comparison; Flame edge validation study using Eq.(12) with velocity as input : (c) amplitude comparison, (d) corresponding phase comparison.

Uniform mixture, 50 m/s, 644K approach flow,
In phase forcing

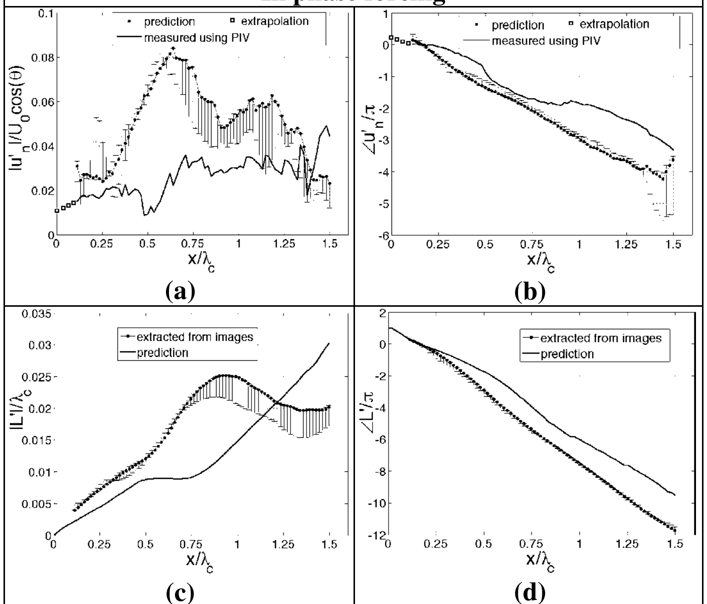

Figure 10. Velocity validation study using Eq.(11) with flame edge as input : (a) amplitude comparison, (b) corresponding phase comparison; Flame edge validation study using Eq.(12) with velocity as input : (c) amplitude comparison, (d) corresponding phase comparison.

Uniform mixture, 50 m/s, 644K approach flow,
Out of phase forcing

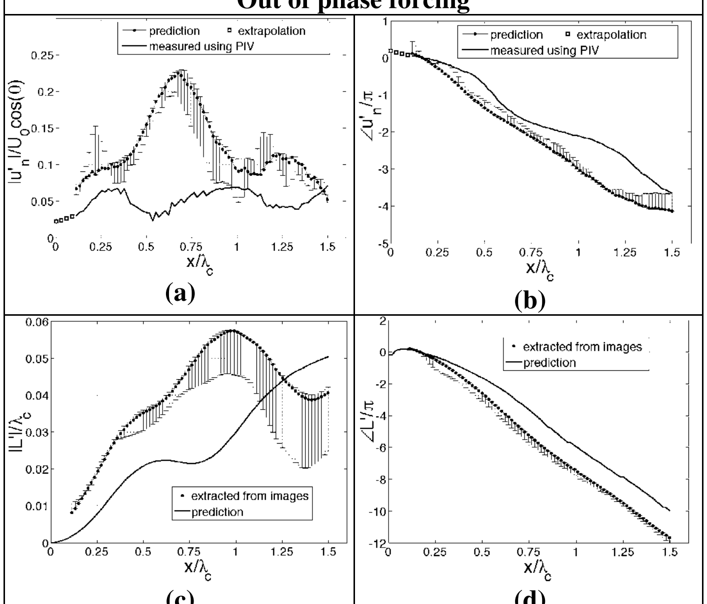

Figure 11. Velocity validation study using Eq.(11) with flame edge as input : (a) amplitude comparison, (b) corresponding phase comparison; Flame edge validation study using Eq.(12) with velocity as input : (c) amplitude comparison, (d) corresponding phase comparison.

Uniform mixture, 100 m/s, 755K approach flow,
In phase forcing

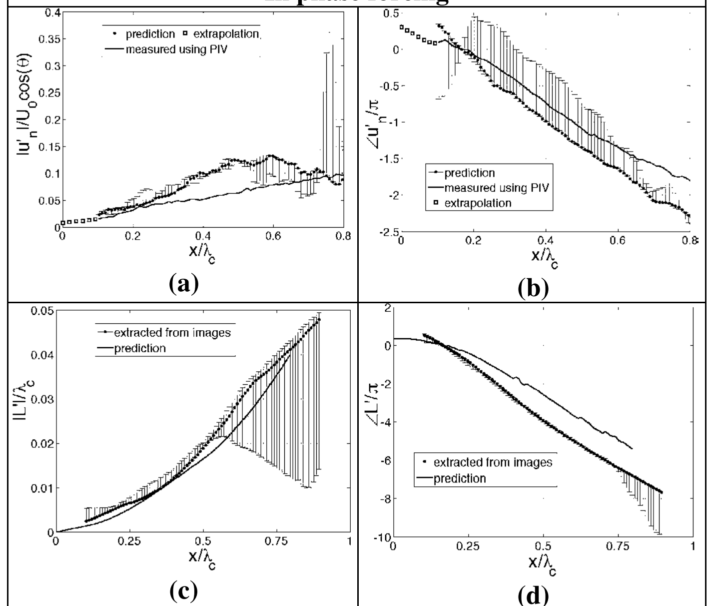

Figure 12. Velocity validation study using Eq.(11) with flame edge as input : (a) amplitude comparison, (b) corresponding phase comparison; Flame edge validation study using Eq.(12) with velocity as input : (c) amplitude comparison, (d) corresponding phase comparison.

Uniform mixture, 100 m/s, 755K approach flow,
Out of phase forcing

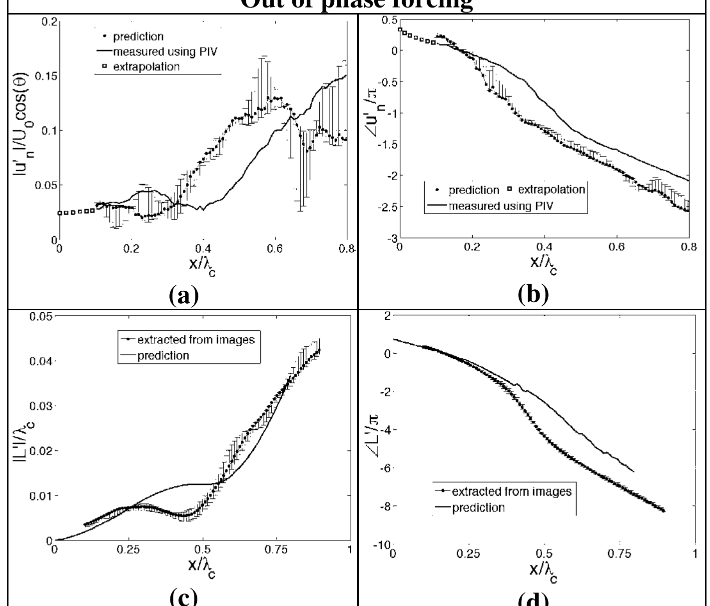

Figure 13. Velocity validation study using Eq.(11) with flame edge as input : (a) amplitude comparison, (b) corresponding phase comparison; Flame edge validation study using Eq.(12) with velocity as input : (c) amplitude comparison, (d) corresponding phase comparison.

Rich on center, 50 m/s, 644K approach flow, In phase forcing

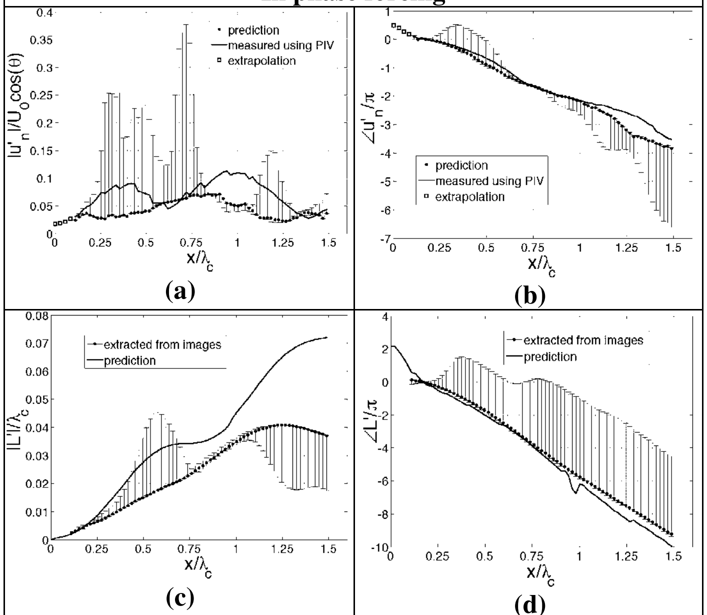

Figure 14. Velocity validation study using Eq.(11) with flame edge as input : (a) amplitude comparison, (b) corresponding phase comparison; Flame edge validation study using Eq.(12) with velocity as input : (c) amplitude comparison, (d) corresponding phase comparison.

Rich on center, 50 m/s, 644K approach flow, Out of phase forcing

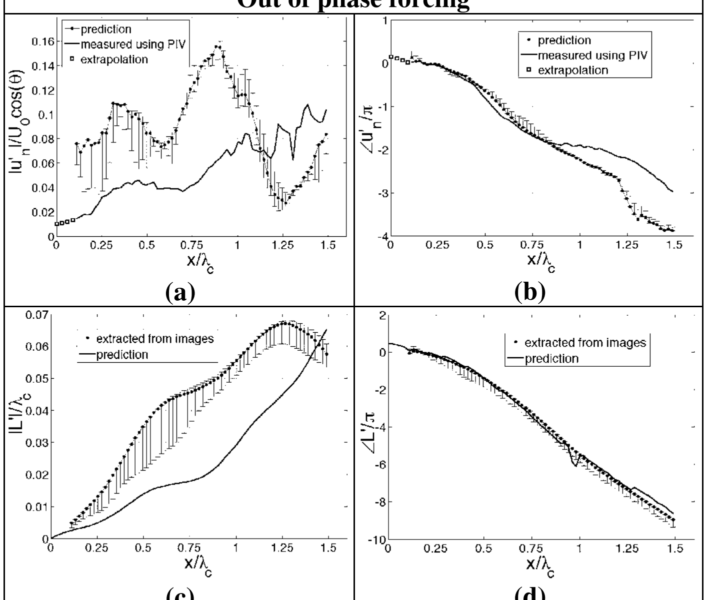

Figure 15. Velocity validation study using Eq.(11) with flame edge as input : (a) amplitude comparison, (b) corresponding phase comparison; Flame edge validation study using Eq.(12) with velocity as input : (c) amplitude comparison, (d) corresponding phase comparison.

Rich on center, 100 m/s, 755K approach flow, In phase forcing

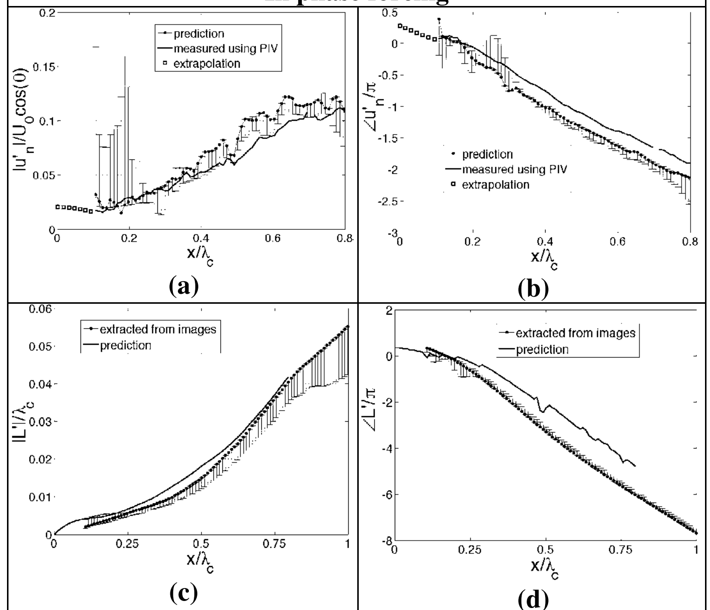

Figure 16. Velocity validation study using Eq.(11) with flame edge as input : (a) amplitude comparison, (b) corresponding phase comparison; Flame edge validation study using Eq.(12) with velocity as input : (c) amplitude comparison, (d) corresponding phase comparison.

Rich on center, 100 m/s, 755K approach flow, Out of phase forcing

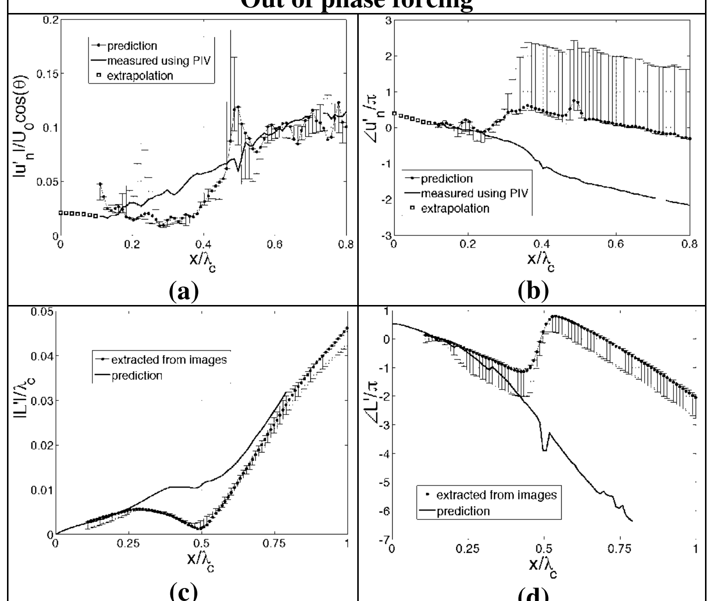

Figure 17. Velocity validation study using Eq.(11) with flame edge as input : (a) amplitude comparison, (b) corresponding phase comparison; Flame edge validation study using Eq.(12) with velocity as input : (c) amplitude comparison, (d) corresponding phase comparison.

CONCLUDING REMARKS

These data show that flame response characteristics at realistic engine conditions can be qualitatively captured from level set based calculations, given suitable knowledge of the disturbance field characteristics. Further work is needed to improve quantitative predictive capabilities, but the discussion in this paper suggests that many of the reasons for disagreement are understood and simply require better time resolved measurements and inclusion of nonlinear effects.

ACKNOWLEDGMENTS

The authors would like to thank the US Air Force (Contract FA-8650-07-M-2784) and the US Department of Energy (Contract DEFG26-07NT43069 and DE-NT0005054, Contract Monitors: Mark Freeman and Richard Wenglarz) for their financial support of this research.

REFERENCES

[1] Smith, D. A., and Zukoski, E. E., 1985, "Combustion Instability Sustained by Unsteady Vortex Combustion," 21st AIAA/ASME/SAE/ASEE Joint Propulsion Conference and Exhibit.

[2] Hegde, U. G., Reuter, D., Daniel, B. R., and Zinn, B. T., 1987, "Flame Driving of Longitudinal Instabilities in Dump Type Ramjet Combustors," Combust. Sci. Technol., 55(4), pp. 125-138.

[3] Poinsot, T. J., Trouve, A. C., Veynante, D. P., Candel, S. M., and Esposito, E. J., 1987, "Vortex-driven acoustically coupled combustion instabilities," J. Fluid Mech., 177, pp. 265-292.

[4] Yu, K. H., Trouvé, A., and Daily, J. W., 1991, "Low-frequency pressure oscillations in a model ramjet combustor," J. Fluid Mech., 232, pp. 47-72.

[5] Hermanson, J. C., and Dimotakis, P. E., 1989, "Effects of Heat Release in a turbulent, reacting shear layer," J. Fluid Mech., 199, pp. 333-375.

[6] Soteriou, M. C., and Ghoniem, A. F., 1994, "The Vorticity Dynamics of an Exothermic, Spatially Developing, Forced Reacting Shear Layer," Proc. Combust. Inst., 25, pp. 1265-1272.

[7] Shanbhogue, S., Shin, D. H., Hemchandra, S., Plaks, D., and Lieuwen, T., 2009, "Flame sheet dynamics of bluff-body stabilized flames during longitudinal acoustic forcing," Proc. Combust. Inst., 32(2), pp. 1787-1794.

[8] Lieuwen, T., Plaks, D. V., and Shin, D.-H., accepted September 2010, "Dynamics of a Longitudinally Forced, Bluff Body Stabilized Flame," J. Propul. Power.

[9] Emerson, B., Acharya, V., Mondragon, U., Brown, C., Shin, D.-H., McDonell, V., and Lieuwen, T., 2011, "Dynamics of a Transversely Forced, Bluff Body Stabilized Flame," 49th AIAA Aerospace Sciences Meeting and ExhibitOrlando, FL, USA.

[10] Schuller, T., Durox, D., and Candel, S., 2003, "A unified model for the prediction of laminar flame transfer functions comparisons between conical and V-flame dynamics," Combust. Flame, 134(1-2), pp. 21-34.

[11] Preetham, Santosh, H., and Lieuwen, T., 2008, "Dynamics of Laminar Premixed Flames Forced by Harmonic Velocity Disturbances," J. Propul. Power, 24(6), pp. 1390-1402.

[12] Shanbhogue, S. J., and Lieuwen, T., 2008, "Studies on the Vorticity Field of Harmonically Excited Bluff Body Flames," 46th AIAA Aerospace Sciences Meeting and Exhibit, Reno, NV, USA.

[13] Louch, D. S., and Bray, K. N. C., 2001, "Vorticity in unsteady premixed flames: vortex pair–premixed flame interactions under imposed body forces and various degrees of heat release and laminar flame thickness," Combust. Flame, 125(4), pp. 1279-1309.

[14] Ducruix, S., Schuller, T., Durox, D., and Candel, S., 2003, "Combustion dynamics and instabilities: Elementary coupling and driving mechanisms," J. Propul. Power, 19(5), pp. 722-734.

[15] Markstein, G. H., 1964, Non-steady flame propagation, Pergamon, New York.

[16] O'Connor, J., Natarajan, S., Malanoski, M., and Lieuwen, T., 2010, "Response of Swirl-Stabilized flames to Transverse Acoustic Excitation," 48th AIAA Aerospace Sciences Meeting and Exhibit, Orlando, FL, USA.

[17] Thumuluru, S. K., and Lieuwen, T., 2009, "Characterization of acoustically forced swirl flame dynamics," Proc. Combust. Inst., 32(2), pp. 2893-2900.

[18] Bellows, B., Neumeier, Y., and Lieuwen, T., 2006, "Forced response of a swirling, premixed flame to flow disturbances," J. Propul. Power, 22(5), p. 1075.

[19] Maxworthy, T., 1962, "On the mechanism of bluff body flame stabilization at low velocities," Combust. Flame, 6, pp. 233-244.

